NASA TM-87754

NASA Technical Memorandum 87754

USAAVSCOM Technical Memorandum 86-B-2

ANALYSIS OF DELAMINATION GROWTH FROM MATRIX CRACKS IN LAMINATES SUBJECTED TO BENDING LOADS

Gretchen Bostaph Murri and E. Gail Guynn

July 1986

NASA
National Aeronautics and Space Administration

Langley Research Center
Hampton, Virginia 23665

Abstract

Delamination is the most commonly observed damage mode in laminated composite materials. A major source of delamination damage is from low-velocity impact. In thin composite laminates under point loads, matrix cracks develop first in the plies, and delaminations then grow from these cracks at the ply interfaces. The purpose of this study was to quantify the combined effects of bending and transverse shear loads on delamination initiation from matrix cracks in composite laminates. Graphite-epoxy laminates with 90° plies on the outside were tested and analysed to provide a two-dimensional simulation of the back-surface damage observed during low-velocity impact. Three plate bending problems were considered: 4-point bending, 3-point bending, and an end-clamped center-loaded plate. Under bending, a matrix crack will form on the tension side of the laminate, through the outer 90° plies and parallel to the fibers. Delaminations will then grow in the interface between the cracked 90° ply and the next adjacent ply. Laminate plate theory was used to derive simple equations relating the total strain energy release rate, G, associated with the delamination growth from a 90° ply crack to the applied bending load and laminate stiffness properties. Three different lay-ups, $[90_4/0/\pm45]_s$, $[90_4/0_3]_s$, and $[90_3/0/\pm45]_s$, were tested and results compared. Test results verified that in all cases the delamination formed at the interface between the cracked 90° ply and the next adjacent ply. Calculated values for total G_c from the analysis showed good agreement for the three lay-ups and the three different test configurations. Using an assumed value for G_{Ic} from a previous study, the analysis was able to predict the delamination onset load for the cases considered. The result indicates that the opening mode component (Mode I) for delamination growth from a matrix crack may be much larger than the component due to interlaminar shear (Mode II).

Nomenclature

a	delamination crack length
A_{11}	laminate extensional stiffness
A_{55}	laminate shear stiffness in xz plane
b	specimen half-width, inches
b_{11}	laminate extension-bending coupling compliance
B_{11}	laminate extension-bending coupling stiffness
d_{11}	laminate bending compliance
D_{11}	laminate bending stiffness
$\bar{S}_{Lam}$	equivalent laminate compliance for original laminate
$\bar{S}_{Del}$	equivalent laminate compliance for sublaminate
E_{11}, E_{22}, G_{12}	lamina moduli
G	total strain energy release rate for delamination
G_I, G_{II}	strain energy release rate components due to interlaminar tension and shear
G_c	critical strain energy release rate for delamination onset
$\bar{g}_{Lam}$	equivalent laminate shear compliance for original laminate
$\bar{g}_{Del}$	equivalent laminate shear compliance for sublaminate
h	laminate thickness
ℓ	specimen half-span, inches
L	moment arm, 4-point bending test, inches
M_x	bending moment per unit width, in-lb/in.
N_{zx}	shear force per unit width, lb/in.
P	applied load, lb.
$\bar{Q}_{11}$	lamina transformed reduced stiffness

U	strain energy of bending
x,y,z	Cartesian coordinates
ε_x	laminate axial strain
κ_x	laminate curvature
ν_{12}	lamina Poisson's ratio
γ_{xz}	laminate shear strain
σ_x	laminate axial stress
τ_{xz}	laminate shear stress

Introduction

As the use of composite materials in primary aircraft structures increases, so must our understanding of failure mechanisms in these materials. The most commonly observed damage mode in composite laminates is delamination damage, which may result from a number of sources. Bostaph and Elber [1,2] observed that for thin composite plates under low-velocity impact, damage begins as local delaminations between plies. The damage is concentrated near the back side of the plate and significant back-face spalling may occur before there is any visible damage on the impacted surface. Typical back-surface damage of a thin graphite-epoxy laminate after low-velocity impact, as simulated by a static indentation test on a clamped circular plate, is shown in Figure 1 where significant ply cracking and spalling are evident. In a recent study, Guynn and O'Brien [3], used a de-ply technique to show that delaminations of impacted regions are always associated with matrix cracking. They observed that matrix cracks will form first through the laminate plies and parallel to the fiber direction. Under bending loads, delaminations will then grow perpendicularly from these cracks where they terminate at ply interfaces. The purpose of this study was to quantify the combined effect of bending and transverse shear loads on delamination initiation from existing matrix cracks in thin laminates.

In order to model a variety of bending situations, three different boundary conditions were considered in the study. A variety of lay-ups was used, each lay-up having 90_n plies on the outsides. The lay-up of the interior of the laminates was varied to provide specimens with different bending stiffnesses. Under bending, a matrix crack will form on the tension side of the laminate, extending through the "n" 90^o plies and parallel to the fibers. Once this matrix crack reaches the interface between the inner-most 90^o ply and the next

adjacent ply, delaminations initiate and grow. In order to isolate the matrix crack and study the problem 2-dimensionally, small coupon specimens were designed to represent the rectangular section shown in Figure 1. Schematic drawings illustrating the three tests and the expected failure are shown in Figure 2. The strain energy release rate associated with this delamination growth can be related to the applied load and laminate stiffness. Simple equations for the strain energy release rate (G) associated with delamination were developed using laminate plate theory. The G values, as determined by the analysis and measured data from T300/5208 graphite epoxy, were compared for a variety of lay-ups and boundary conditions.

Procedure

Small (5 inch by 1 inch) specimens of T300/5208 graphite-epoxy were tested in the study. Three lay-ups, $[90_4/0/\pm45]_s$, $[90_4/0_3]_s$, and $[90_3/0/\pm45]_s$ were chosen for testing. These lay-ups were selected to provide test specimens with different laminate stiffnesses, but with the delamination confined to the [90/0] interface. All specimens were manufactured at NASA Langley. The $[90_4/0/\pm45]_s$ and $[90_4/0_3]_s$ lay-ups were cured in a press while the $[90_3/0/\pm45]_s$ lay-up was cured in an autoclave. The different curing processes yielded a fiber volume fraction (V_f) of 70% for the pressed panels and a V_f of 61% for the autoclaved panel. The specimen configuration for the bending tests is shown in Figure 3. In order to study delamination initiation from pre-existing matrix cracks, and to be able to isolate the crack, specimens were tested with simulated matrix cracks. These simulated precracks were formed in two different ways, either by carefully cutting through the outside 90^o plies to the [90/0] interface with a razor blade, or by having the specimens manufactured with a thin (1 mil) Mylar

strip at the mid-span through the 90^{o} plies on one side of the laminate. When razor precracks were used they were first examined under a light microscope to verify that the razor cut extended to the [90/0] interface but not into the 0^{o} ply.

Three different bending conditions were chosen. To simulate pure bending, specimens were loaded across their width in a 4-point bending test. A 3-point bending test was used to include the effects of transverse shear forces. Conditions similar to low-velocity impact of a laminate near a rigid support were simulated by clamping the specimens at the ends and loading them across their width at the mid-span.

The 4- and 3-point bending test apparatuses are shown in Figures 4 and 5, respectively. These two fixtures are similar in design, both using rollers to apply the loads across the specimen width. The loading pins are 0.25-inch diameter steel rods. Annular ball bearings were positioned at each end of the loading pins and supported in U-shaped aluminum channels as shown. This combination of loading pins and annular ball bearings created a roller system and thus, simply-supported conditions. In the 4-point bend test, the inside and outside span lengths were 3 and 4 inches, respectively. The span of the three-point bend test was 3 inches with the load applied at the midspan of the specimen.

The end-clamped, center-loaded test apparatus is shown in Figure 6. Clamped boundary conditions were obtained by clamping one square inch of each end of the specimen between two aluminum plates as shown. The span between the clamps was 3 inches. The specimens were loaded across their midspan width with a one-inch wide wedge. For all tests, loads were applied with a servo-controlled hydraulic test stand. The specimens were loaded in displacement control at a rate of .08 in./min, until the delamination grew. In all cases the

initial growth was very rapid, extending the crack about one-half inch on each side of the precrack. Center point displacements were measured with a direct current displacement transducer (DCDT) whose rod was supported by a spring as shown in Figures 4 and 5. The load-displacement behavior of the specimen was recorded on an x-y plotter. Typical load-displacement results for a $[90_4/0_3]_s$ laminate in 4-point bending and end-clamped bending conditions are shown in Figure 7. The load-deflection plots were linear to the onset and growth of delamination for the end-clamped tests for all lay-ups. The 4-point bending and 3-point bending tests exhibited some small amount of non-linearity in nearly all cases before delamination occurred. This non-linearity was attributed to the test fixtures and was small enough that it was not a concern.

Analysis

Simple equations for the strain energy release rate associated with delamination growth, under a constant out-of-plane displacement, from a matrix crack were developed for each bending configuration using a strain energy release rate definition of the form

$$G = \frac{dW}{dA} - \frac{dU}{dA} \tag{1}$$

where A is the surface area created by the delamination, W is the work performed by the external loads, U is the strain energy, which in general is given in terms of the laminate stresses by

$$U = \frac{1}{2}\int(\sigma_x\varepsilon_x + \sigma_y\varepsilon_y + \sigma_z\varepsilon_z + \tau_{xy}\gamma_{xy} + \tau_{xz}\gamma_{xz} + \tau_{yz}\gamma_{yz})dV \tag{2}$$

and $W=2U$

For the three bending configurations considered, equation (2) can be reduced to

$$U=\frac{1}{2}\int_V (\sigma_x\varepsilon_x + \tau_{xz}\gamma_{xz})dV \tag{3}$$

The axial strain and stress in the k^{th} ply are given by laminated plate theory [4] as

$$\varepsilon_x = \varepsilon_x^o + z\kappa_x \tag{4}$$

$$\sigma_x = \bar{Q}_{11}\varepsilon_x \tag{5}$$

where ε_x^o and κ_x are the midplane strains and curvatures in the x direction respectively, and $\bar{Q}_{11}$ is the transformed reduced stiffness. The transverse shear stress in the k^{th} ply is given by

$$\tau_{xz} = \bar{Q}_{55}\gamma_{xz} \tag{6}$$

Substituting eqs. (4-6) into eq.(3) yields

$$U=\frac{1}{2}\iiint \sum_{k=1}^{N} \int_{z_{k-1}}^{z_k} [(\bar{Q}_{11}\varepsilon_x^{o\,2} + 2\bar{Q}_{11}z\varepsilon_x^o\kappa_x + z^2\bar{Q}_{11}\kappa_x^2)_k + (\bar{Q}_{55}\gamma_{zx}^2)_k] \, dx \, dy \, dz \tag{7}$$

where N is the number of plies in the laminate, γ_{zx} is the shear strain in the zx plane and z_k is the distance from the midplane to the k^{th} ply. Performing the integration and summing in the z direction, eq. (7) becomes

$$U=\frac{1}{2}\iint [(A_{11}\varepsilon_x^{o\,2} + 2B_{11}\kappa_x\varepsilon_x^o + D_{11}\kappa_x^2) + (A_{55}\gamma_{xz}^2)] \, dx \, dy \tag{8}$$

where A_{11}, B_{11}, D_{11}, and A_{55} are the laminate extensional, bending-extension coupling, bending, and transverse shear stiffnesses, respectively. The terms ε_x^o, κ_x, and γ_{xz} can be expressed in terms of the external loads as

$$\begin{aligned} \varepsilon_x^o &= b_{11}M_x \\ \kappa_x &= d_{11}M_x \\ \gamma_{zx} &= \frac{N_{zx}}{hG_{zx}} \end{aligned} \tag{9}$$

where b_{11} and d_{11} are compliances for bending-extension coupling and bending, respectively, as defined by laminate plate theory [4]. M_x and N_{xz} represent the applied moment and shear load per unit width for the particular bending configuration of interest. Substituting equations (9) into equation (8), and integrating in the y-direction results in

$$U=\frac{(2b)}{2}\int \{(A_{11}b_{11}^2 + 2B_{11}b_{11}d_{11} + D_{11}d_{11}^2)M_x^2 + (\frac{A_{55}}{h^2G_{zx}^2})N_{xz}^2\}dx \quad (10)$$

where it should be noted that, in general, $B_{11}\neq\frac{1}{b_{11}}$ and $D_{11}\neq\frac{1}{d_{11}}$.

Moment and shear diagrams for the three bending problems considered here are shown in Figure 8. The 4-point bending test provides pure bending (i. e., no transverse shear forces) between the inner load points. The 3-point bend test has a linearly varying moment which is a maximum at the midspan and has a constant shear force through the test section. The clamped end condition has the same constant transverse shear force, and a moment which is negative at the supports, zero at the quarter-span points and maximum at the mid-span. The moment and shear expressions for the three cases are

A. Four-point bending

$$M_x=\frac{PL}{4b} \quad \text{where } L\leq x\leq(2\ell-L) \quad (11)$$

$$N_{xz}=0 \quad (12)$$

B. Three-point bending

$$M_x=\frac{Px}{4b} \quad \text{where } 0\leq x\leq\ell \quad (13)$$

$$N_{xz}=\frac{P}{4b} \quad (14)$$

C. End-clamped

$$M_x=\frac{P}{8b}(2x-\ell) \quad \text{where } 0\leq x\leq\ell \quad (15)$$

$$N_{xz}=\frac{P}{4b} \quad (16)$$

The half-span of the laminate can be modelled as a laminated region and a sublaminate created by the growth of the delamination as shown in Figure 9 for the three point bending case. This sublaminate is an asymetric laminate consisting of the original laminate minus the cracked 90^o plies that are delaminated and no longer carry load. Equation (3) can therefore be expressed as

$$U=U_{Lam} + U_{Del} \quad (17)$$

where the subscripts Lam and Del refer to the laminate and sublaminate respectively. By using the appropriate equations for the bending moment M_x and transverse shear N_{xz} for the particular configuration of interest, equation (10) can then be integrated over the half-span. For the complete laminate this expression must be multiplied by 2, to yield an expression for the strain energy of the laminate in terms of the laminate constants, the applied load and the crack length a. For simplicity, let

$$\bar{S} = A_{11}b_{11}^2 + 2B_{11}b_{11}d_{11} + D_{11}d_{11}^2 \tag{18}$$

and

$$\bar{g} = \frac{A_{55}}{h^2 G_{xz}^2} \tag{19}$$

It is then possible to calculate $\bar{S}_{Del}$, $\bar{g}_{Del}$ for the sublaminate and $\bar{S}_{Lam}$, $\bar{g}_{Lam}$ for the laminated region. Using equations (11-16) and (18-19) and substituting equation (10) into equation (1) and differentiating, where A is the total delaminated area and dA=(2b)2(da), the following three equations can be determined for the total strain energy release rate for the 4-point bending, 3-point bending and end-clamped configurations, respectively.

$$G = \frac{P^2L^2}{32b^2}(\bar{S}_{Del} - \bar{S}_{Lam}) \tag{20}$$

$$G = \frac{P^2}{32b^2}[(\ell^2 - 2\ell a + a^2)(\bar{S}_{Del} - \bar{S}_{Lam}) + (\bar{g}_{Del} - \bar{g}_{Lam})] \tag{21}$$

$$G = \frac{P^2}{32b^2}[(\frac{\ell^2}{4} - \ell a + a^2)(\bar{S}_{Del} - \bar{S}_{Lam}) + (\bar{g}_{Del} - \bar{g}_{Lam})] \tag{22}$$

where P is the load, and L, b, and ℓ are specimen geometry terms as defined in Figure 2. In the calculations G_{xz} was assumed to be approximately equal to G_{xy} according to [5].

In Figure 10, G is plotted for equations (20), (21), and (22), as a function of normalized delamination length, a/ℓ, for a $[90_4/0/\pm45]_s$ laminate

with a unit load. Figure 10 shows that for the 4-point bending case G is constant and independent of a, and for the 3-point bending and the end-clamped cases a maximum value of G occurs when the delamination length, a, approaches zero. Figure 10 also shows that for the 3-point bending and end-clamped cases, G reaches a minimum value which is very close to zero. This minimum G value represents the transverse shear component only. As the figure clearly demonstrates, the transverse shear contribution (which is not a function of a) is very small compared to the bending component. For the purposes of this study, the influence of the interlaminar normal and shear stress singularity associated with the existing matrix crack is not considered. The G values calculated from equations (20-22) are based on net section stresses and strains in each ply. A boundary value problem must be formulated and solved to determine the nature of the interlaminar stress singularity, and the manner in which G reaches the values obtained from equations (20-22) as the crack forms. In the absence of this rigorous solution, it was assumed that the values of G in equations (20-22) as $a \to 0$ are maxima. When a value of $a=0$ is substituted in equations (20), (21), and (22), they become

$$G=\frac{P^2L^2}{32b^2}(\bar{S}_{Del}-\bar{S}_{Lam}) \tag{23}$$

$$G=\frac{P^2}{32b^2}[\ell^2(\bar{S}_{Del}-\bar{S}_{Lam})+(\bar{g}_{Del}-\bar{g}_{Lam})] \tag{24}$$

$$G=\frac{P^2}{32b^2}[\frac{\ell^2}{4}(\bar{S}_{Del}-\bar{S}_{Lam})+(\bar{g}_{Del}-\bar{g}_{Lam})] \tag{25}$$

The critical load measured at delamination onset P_c, was substituted into equations (23-25) to determine the critical strain energy release rates, G_c for onset of the delamination from the matrix crack.

Test data and calculated G_c values are given in Tables 1, 2, and 3 for the 4-point bending, 3-point bending, and clamped center-loaded

configurations, respectively. The specific ply properties used to compute the laminate stiffnesses for the T300/5208 material were

$$E_{11} = 19.5 \times 10^6 \quad \text{psi}$$
$$E_{22} = 1.48 \times 10^6 \quad \text{psi} \qquad (26)$$
$$G_{12} = .8 \times 10^6 \quad \text{psi}$$
$$\nu_{12} = 0.3$$

Calculated compliance terms based on these assumed properties are shown in Table 1 for the 4-point bending tests, along with the actual measured bending compliances from testing. The agreement is good for the three lay-ups.

Results and Discussion

A typical failed specimen is shown in Figure 11 for the four-point bending configuration. The figure clearly shows that the delamination grew symmetrically from the simulated matrix crack and the nature of the failure indicates that it may be a mode I or peel failure. Light microscopy was used to verify that the bending load did result in a delamination at the [90/0] interface and did not cause cracking through the 0° ply or extensive fiber bridging. Figure 12 shows a detailed view of the delamination growth from a simulated matrix crack in a $[90_4/0_3]_s$ laminate, as seen through a light microscope. The delamination surface is clearly indicated in this figure at the [90/0] interface. A scanning electron microscope (SEM) was used to examine the delaminated surfaces of selected specimens to determine whether the delamination was occurring in the matrix material and whether any fiber bridging was present. The failure surfaces were also carefully examined by means of a scanning electron microscope (SEM). Figure 13a shows an SEM micrograph for one such failure surface at 65X magnification. The absence of 0° fibers on this surface indicates that the delamination started and grew at the [90/0] interface.

Figure 13b is a higher 1000X magnification of the area at the crack tip. This micrograph shows that the remaining matrix material adhered to the 90^{o} fibers. This matrix material contains imprints from the 0^{o} fibers in the adjacent ply, which again indicates that the delamination occurred at the [90/0] interface. Neither micrograph shows any indication of fiber bridging at a≈0, although there was a tendency to pick up fibers as the crack extended further. In this study, however, we are concerned only with the behavior at a≈0, where there was no evidence of fiber bridging. SEM examination was used to verify that the delamination always formed and grew at the [90/0] interface regardless of lay-up, test configuration, or type of pre-crack used.

Failure loads and specimen geometries for the three laminates and three test configurations are given in Tables 1, 2, and 3. The calculated G_c values for each test configuration are shown graphically in Figure 14 for each test lay-up. These values were calculated using equations (23-25) and the measured failure loads. Figure 14 shows that for a given lay-up there is little variation in G_c for the different tests, although the results from the clamped end conditions are always slightly higher. For the 3-point bend test results are shown for the $[90_4/0_3]_s$ laminate using both a razor pre-crack and a Mylar insert. The results differ only slightly for the two methods indicating little effect due to the sharpness (or bluntness) of the initial matrix crack tip. Both techniques seem reasonable for simulating an initial crack. Figure 15 shows a comparison of results of the different lay-ups for each type of test. Figure 15 shows little variation of results for any of the lay-ups using the 4-point bend test where there is no transverse shear. The 3-point bending and end-clamped tests yielded similar results for the two 14-ply laminates.Slightly higher values were observed for the 12-ply, $[90_3/0/\pm 45]_s$ lay-up. This may be due in part to the lower fiber volume fraction (61%) of that panel compared to

the 14-ply panels (70%). This difference may also be due to different percentages of the failure modes, interlaminar tension (mode I) and in-plane shear (mode II) occurring in the different lay-ups. A finite element analysis will be required to accurately determine the mode breakdowns in these laminates.

In [6], Wilkins, et al used double-cantilevered beam tests (DCB) to measure the Mode I critical strain energy release rate of T300/5208 graphite-epoxy. Their results give a value of $G_c=0.5\ \frac{in\text{-}lb}{in^2}$ where $G_c=G_{I_c}$ since the DCB is a pure Mode I test. Similarly, in [7] O'Brien conducted edge-delamination tests on $[\pm 30/\pm 30/90_2]_s$ laminates of T300/5208 where G_c was measured and the G_{Ic} component was calculated from finite element analysis. Those results also indicated a value of G_{Ic} of approximately $0.5\ \frac{in\text{-}lb}{in^2}$. A comparison of the present results for G_c with the G_{Ic} results from these previous studies indicates that for these bending tests, the failure is likely a predominantly Mode I event. Using a value of $G=0.5\ \frac{in\text{-}lb}{in^2}$ in equations (23-25), failure loads were predicted for the three lay-ups and test configurations. The results are plotted in Figure 16, where the symbols represent the predicted failure loads and the bands represent the range of the actual test data. For almost all cases the predicted failure was within the range of the actual measured failure loads but tended to be near the high end of the range. The figure demonstrates that a good prediction can be made of the failure load by using the mode I strain energy release of the material. This again emphasizes that for the laminates considered here, under bending loads the delamination initiation is likely to have a large opening component and is not strongly affected by the transverse shear load.

Conclusions

In this study graphite-epoxy laminates with 90° plies on the outside were used to two-dimensionally simulate the back-surface damage observed during low-velocity impact of composite plates. Three different plate bending problems were considered: 4-point bending, 3-point bending, and an end-clamped, center loaded plate. These bending configurations were analyzed using laminate plate theory and simple equations were derived relating the total strain energy release rate , G_c, associated with the delamination growth from a 90° ply crack to the applied bending load and laminate stiffness properties. For each bending problem, three different lay-ups were tested and results compared. Results of the analysis and testing indicate that:

1. Delaminations formed at the interface where the matrix crack terminated and appeared to have a significant crack opening displacement.
2. A G analysis based on laminated plate theory was derived. Total G_c values determined from this analysis and measured applied loads at delamination onset from the matrix crack yielded similar results for all three layups and bending configurations studied.
3. The contribution of the transverse shear to the total G_c was very small for the three-point bending and end-clamped cases.
4. Measured G_c values were similar to G_{Ic} values for the same material, as measured by DCB and EDT tests. Hence, delamination from matrix cracks in laminates subjected to bending loads appears to be predominantly a Mode I phenomenon.

References

1. Bostaph, G. M., and Elber, W., "Static Indentation Tests on Composite Plates for Impact Susceptibility Evaluation." Proceedings of the Army Symposium on Solid Mechanics, 1982 - Critical Mechanics Problems in Systems Design, AMMRC MS 82-4, U.S. Army, September 1982, pp. 288-317.

2. Bostaph, G. M., and Elber, W., "A Fracture Mechanics Analysis for Delamination Growth During Impact on Composite Plates," 1983 Advances in Aerospace Structures, Materials and Dynamics; Proceedings of the ASME Annual Meeting, pp. 133-138.

3. Guynn, E. G., and O'Brien, T. K., "The Influence of Lay-up and Thickness on Composite Impact Damage and Compression Strength," Proceedings of the AIAA/ASME/ASCE/AHS 26th Structures, Structural Dynamics, and Materials Conference, April 1985, Orlando, FL, pp. 187-196.

4. Jones, R. M., Mechanics of Composite Materials, McGraw-Hill Book Co., New York, 1975.

5. Kriz, R. D., and Stinchcomb, W. W., "Elastic Moduli of Transversely Isotropic Graphite Fibers and Their Composites," Experimental Mechanics, Volume 19, Feb. 1979, pp. 41-49.

6. Wilkins, D. J., Eisenmann, J. R., Camin, R. A., Margolis, W. S., and Benson, R. A., "Characterizing Delamination Growth in Graphite-Epoxy," Damage in Composite Materials, ASTM STP 775, 1982, pp. 168-183.

7. O'Brien, T. K., Johnston, N. J., Raju, I. S., Morris, D. H., and Simonds, R. A., "Comparisons of Various Configurations of the Edge Delamination Test for Interlaminar Fracture Toughness", NASA TM 86433, July 1985.

Table Titles

Table 1. Four-point bending test results.

Table 2. Three-point bending test results.

Table 3. End-clamped, center-loaded test results.

Figure Captions

Figure 1. Back-surface damage due to out-of-plane loading.

Figure 2. Bending test configurations.

Figure 3. Specimen configuration.

Figure 4. Four-point bending apparatus.

Figure 5. Three-point bending apparatus.

Figure 6. Clamped, center-loaded apparatus.

Figure 7. Load-deflection plots for $[90_4/0_3]_s$ laminate.

Figure 8. Shear and moment diagrams for three test configurations.

Figure 9. Laminate-sublaminate bending model.

Figure 10. G_c vs. normalized delamination length for three bending configurations.

Figure 11. Matrix crack induced delamination.

Figure 12. Delaminated [90/0] interface in $[90_4/0_3]_s$ laminate.

Figure 13. [90/0] failure surface for a $[90_4/0_3]_s$ laminate.

Figure 14. G_c results for three lay-ups and three test configurations.

Figure 15. G_c results for three test configurations and three lay-ups.

Figure 16. Predicted and measured G_c results for three lay-ups and three bending configurations.

Table 1

Lay-up	b,in	h,in	l,in	Pc,lbs	G_c, $\frac{in\text{-}lb}{in^2}$	C X 10^3 $\frac{in}{lb}$ measured	C X 10^3 $\frac{in}{lb}$ calculated
$[90_4/0/\pm 45_s]$	.4970	.0739	.5	48	.353	3.75	3.22
	.4970	.0760	.5	50	.384	3.15	3.22
	.4971	.0765	.5	46	.325	2.4	3.22
	.4970	.0757	.5	57	.498	3.38	3.22
	.4978	.0772	.5	47	.338	3.46	3.21
	.4978	.0763	.5	51	.398	3.5	3.21
$[90_4/0_3]_s$	.4983	.0600	.5	38	.296	3.33	2.80
	.4973	.0630	.5	44	.398	3.43	2.81
	.4980	.0600	.5	43.5	.388	3.2	2.81
	.4985	.0602	.5	46.5	.443	3.0	2.80
	.4989	.0601	.5	37	.280	3.2	2.8
	.4988	.0600	.5	49	.491	3.25	2.8
	.4991	.0600	.5	48	.470	3.17	2.8
$[90_3/0/\pm 45_s]$	.4964	.0688	.5	66.5	.491	3.67	3.03
	.4960	.0702	.5	62	.427	4.2	3.03
	.4956	.0714	.5	67	.500	3.86	3.03
	.4964	.0710	.5	66.5	.491	3.86	3.03
	.4968	.0683	.5	56	.347	3.0	3.03
	.4907	.0713	.5	60	.409	4.1	3.06
	.4962	.0715	.5	66	.484	3.9	3.06

Table 2

Lay-up	b,in	h,in	l,in	Pc,lbs	G_c,$\frac{in\text{-}lb}{in^2}$
$[90_4/0/\pm45]_s$	.4994	.0741	1.5	14	.287
	.4998	.0743	1.5	17.5	.448
	.4996	.0742	1.5	17.5	.448
	.4973	.0755	1.5	15	.310
	.4975	.0754	1.5	16.5	.375
	.4975	.0755	1.5	18	.447
	.4975	.0768	1.5	14	.270
	.4977	.0766	1.5	16	.352
$[90_4/0_3]_s$	.4982	.0728	1.5	21	.407
	.4984	.0746	1.5	20	.369
	.4971	.0769	1.5	19	.335
$[90_4/0_3]$ with Mylar	.5048	.0714	1.5	17	.296
	.5052	.0715	1.5	18	.331
	.5057	.0710	1.5	18	.330
$[90_3/0/\pm45]_s$	.4906	.0691	1.5	24	.575
	.4953	.0700	1.5	22	.486
	.4967	.0719	1.5	20	.399
	.4966	.0702	1.5	22.5	.505
	.4964	.0692	1.5	24	.575
	.4957	.0715	1.5	24	.577
	.4963	.0707	1.5	22	.484

Table 3

Lay-up	b,in	h,in	l,in	Pc,lbs	G_c,$\frac{in\text{-}lb}{in^2}$
$[90_4/0/\pm 45]_s$	.5000	.0746	1.5	46	.773
	.5000	.0750	1.5	42	.645
	.4994	.0754	1.5	29	.308
	.4976	.0759	1.5	32.5	.364
	.4978	.0758	1.5	28	.270
	.4979	.0754	1.5	38	.497
	.4978	.0772	1.5	33	.375
	.4972	.0765	1.5	41	.581
	.4980	.0759	1.5	36.5	.459
$[90_4/0_3]_s$	.4984	.0729	1.5	37	.316
	.4981	.0748	1.5	43.5	.438
	.4986	.0744	1.5	48.5	.543
	.4982	.0766	1.5	45.5	.479
	.4986	.0727	1.5	42.5	.979
$[90_3/0/\pm 45]_s$	.4964	.0720	1.5	43.5	.473
	.4903	.0696	1.5	50	.641
	.4964	.0707	1.5	54	.729
	.4970	.0714	1.5	44	.483
	.4966	.0715	1.5	49	.599
	.4968	.0697	1.5	44	.483

Figure 1. Back-surface damage due to out-of-plane loading.

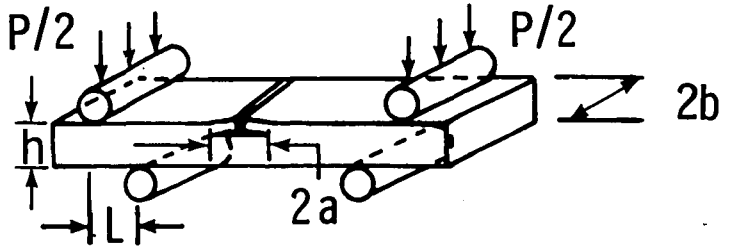

(a) 4-point bending

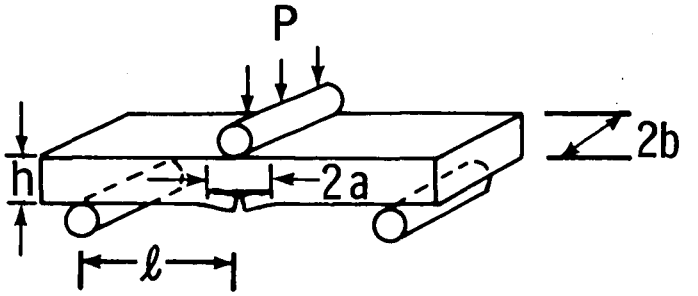

(b) 3-point bending

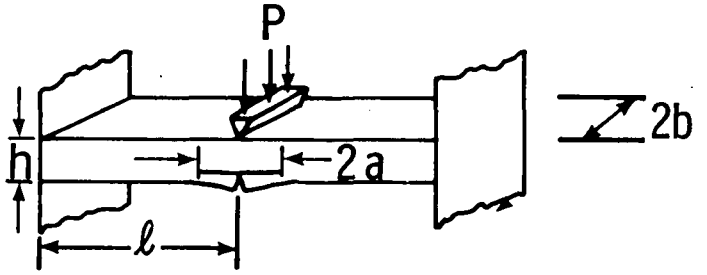

(c) End-clamped center-loaded bending

Figure 2. Bending test configurations.

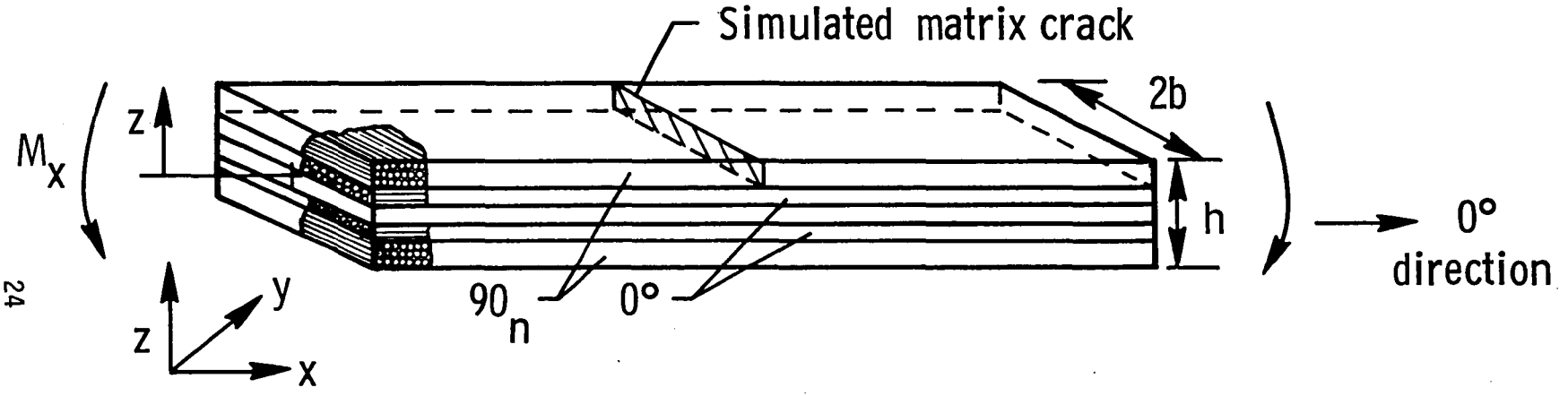

Figure 3. Specimen configuration.

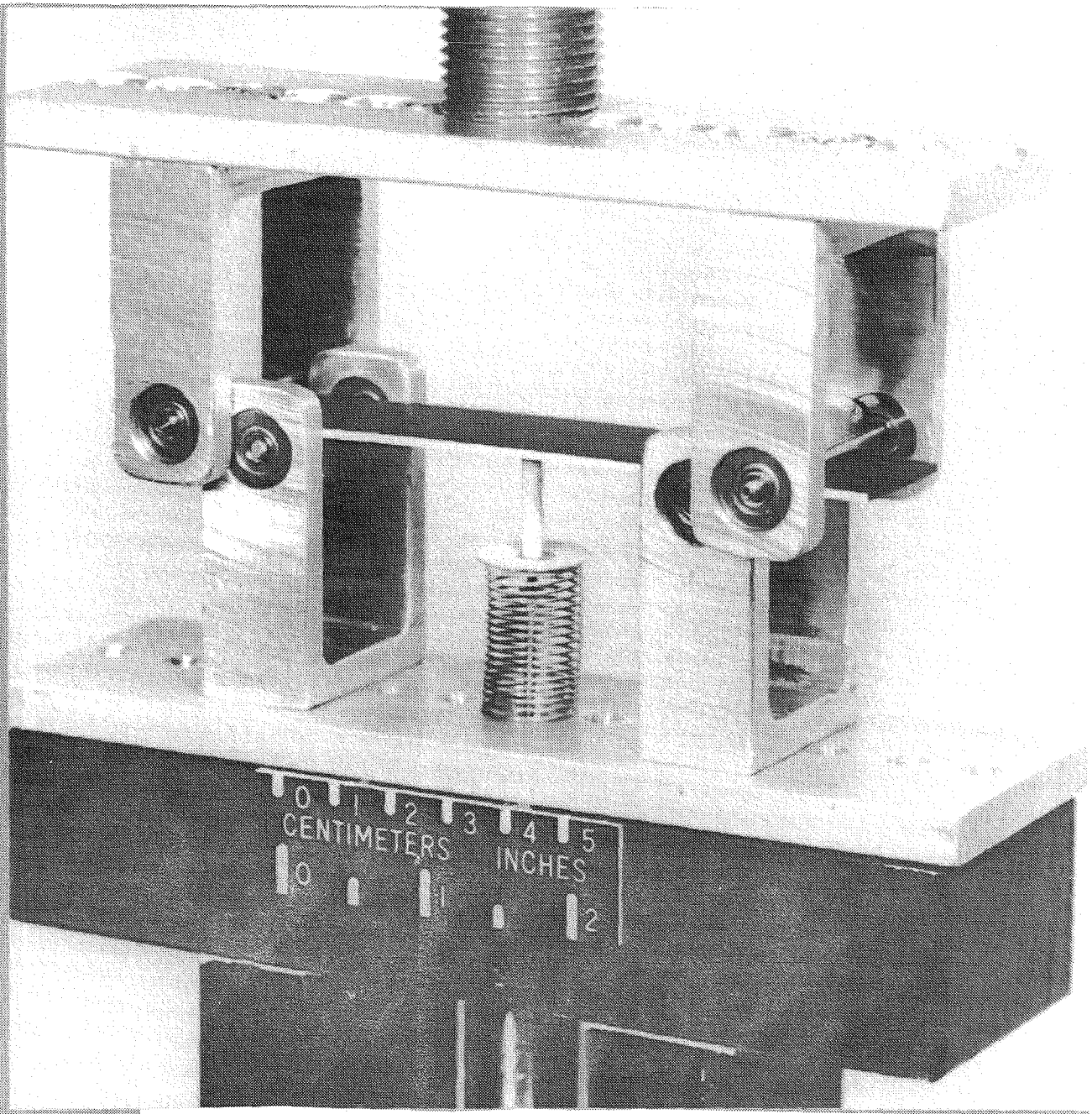

Figure 4. Four-point bending apparatus.

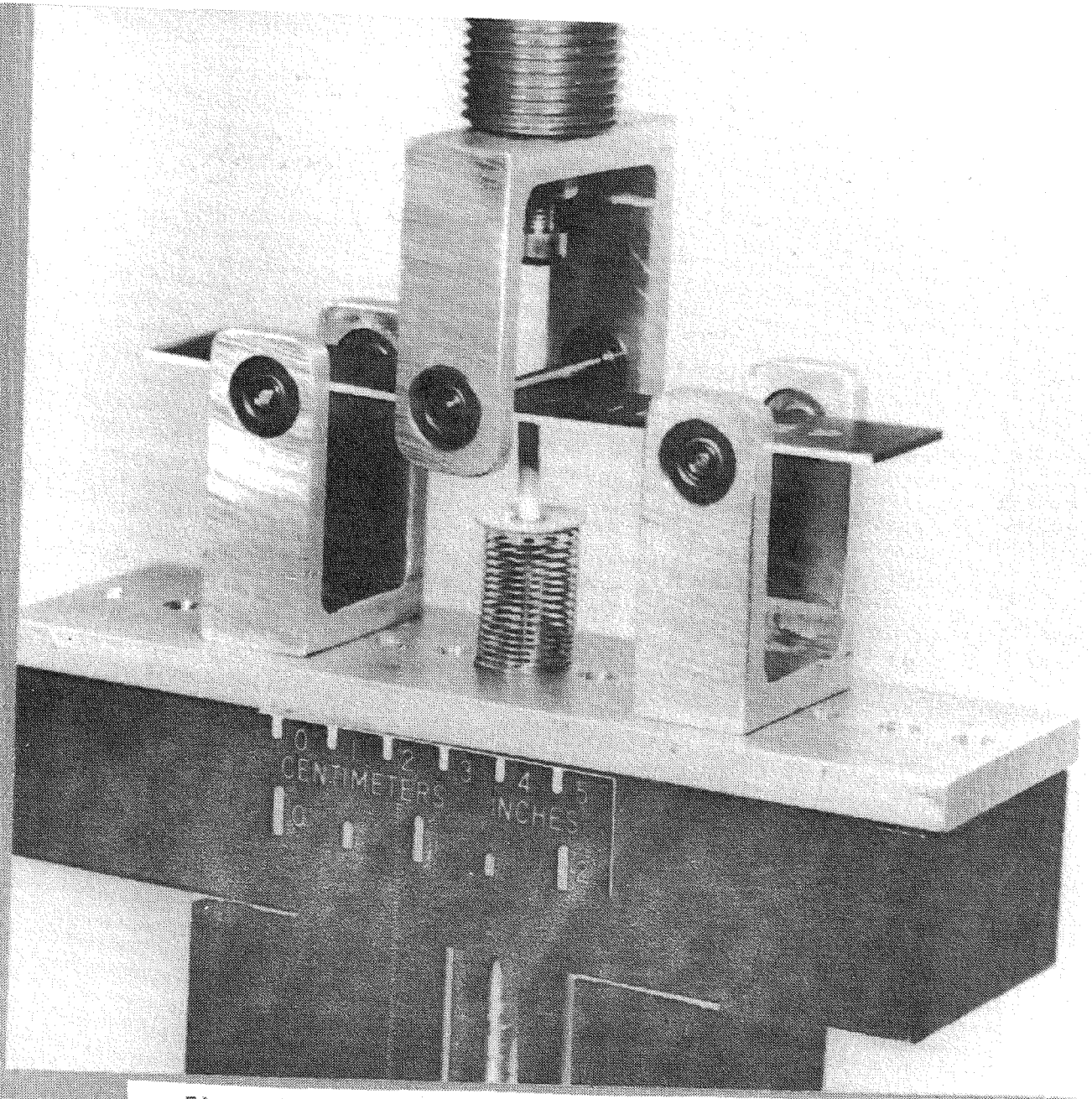

Figure 5. Three-point bending apparatus.

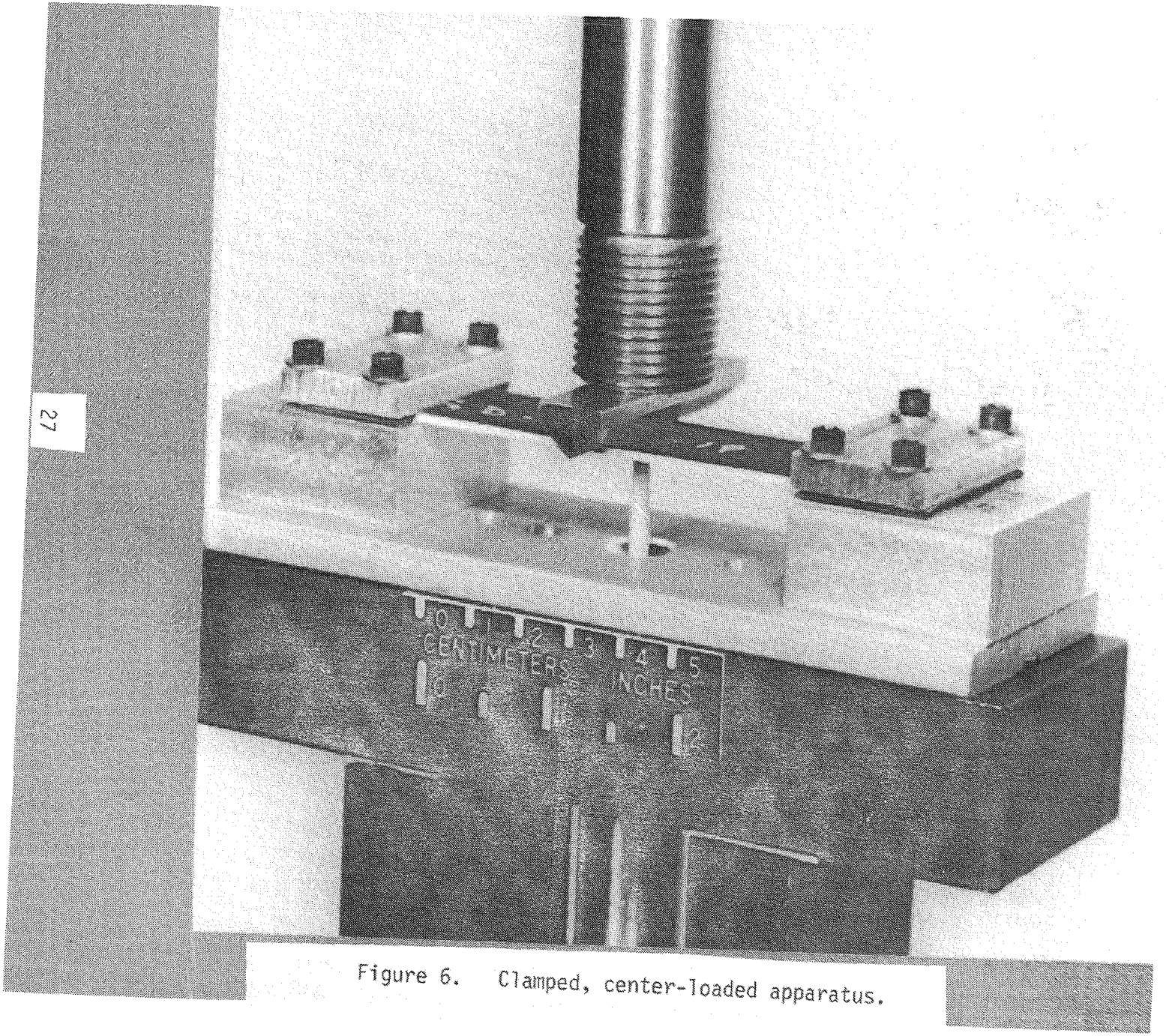

Figure 6. Clamped, center-loaded apparatus.

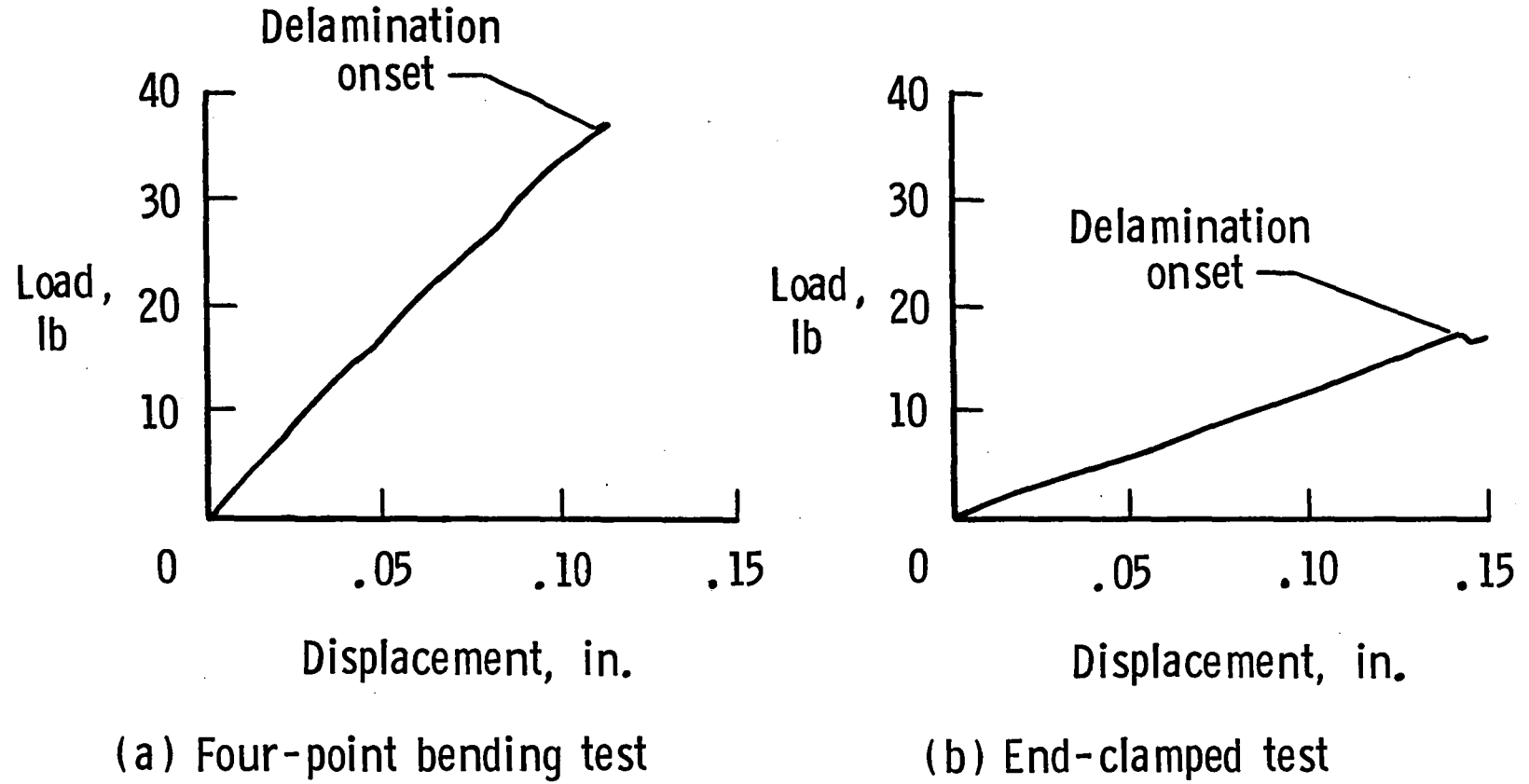

Figure 7. Load-deflection plots for $[90_4/0_3]_s$ laminate.

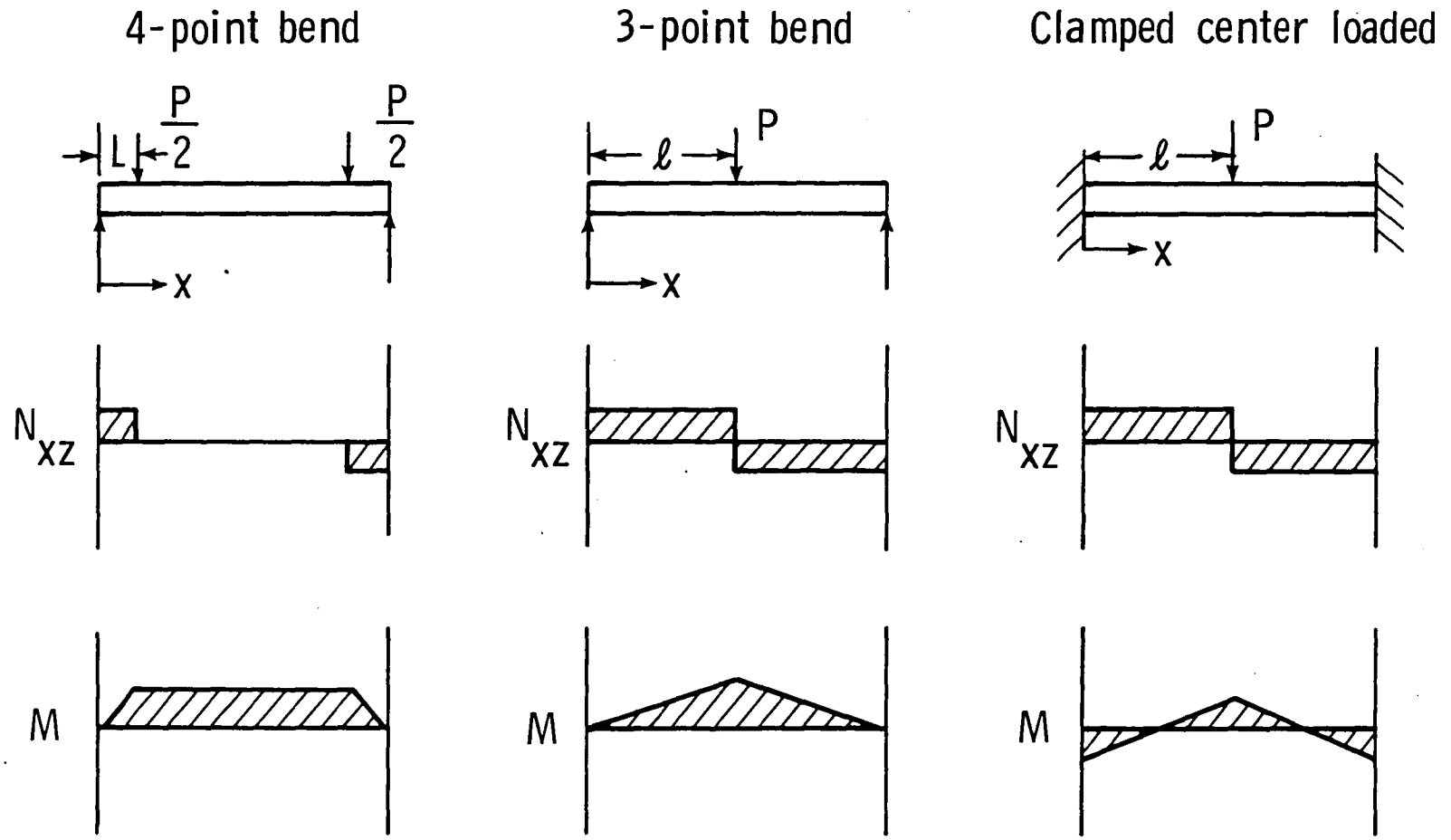

Figure 8. Shear and moment diagrams for three test configurations.

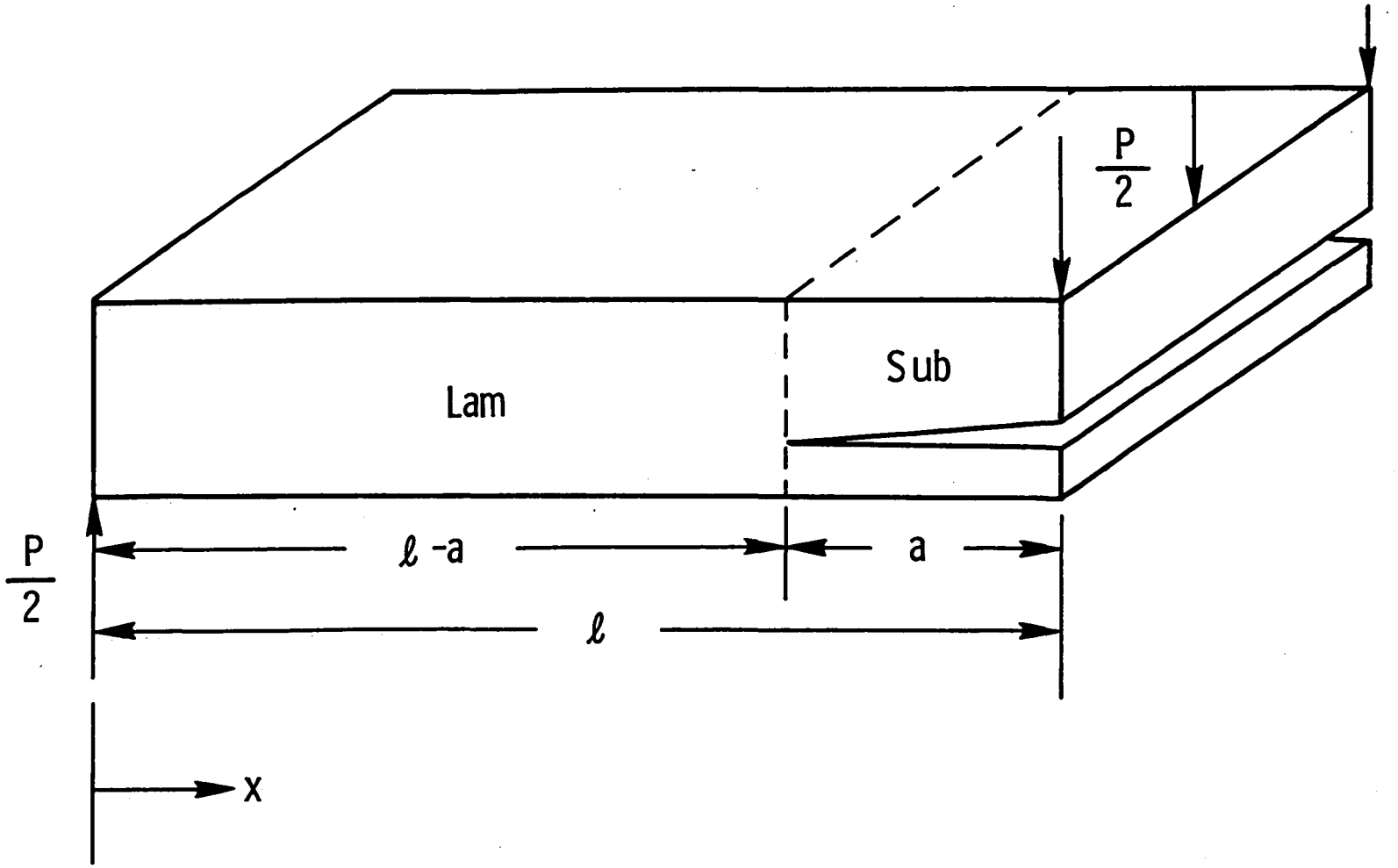

Figure 9. Laminate-sublaminate bending model.

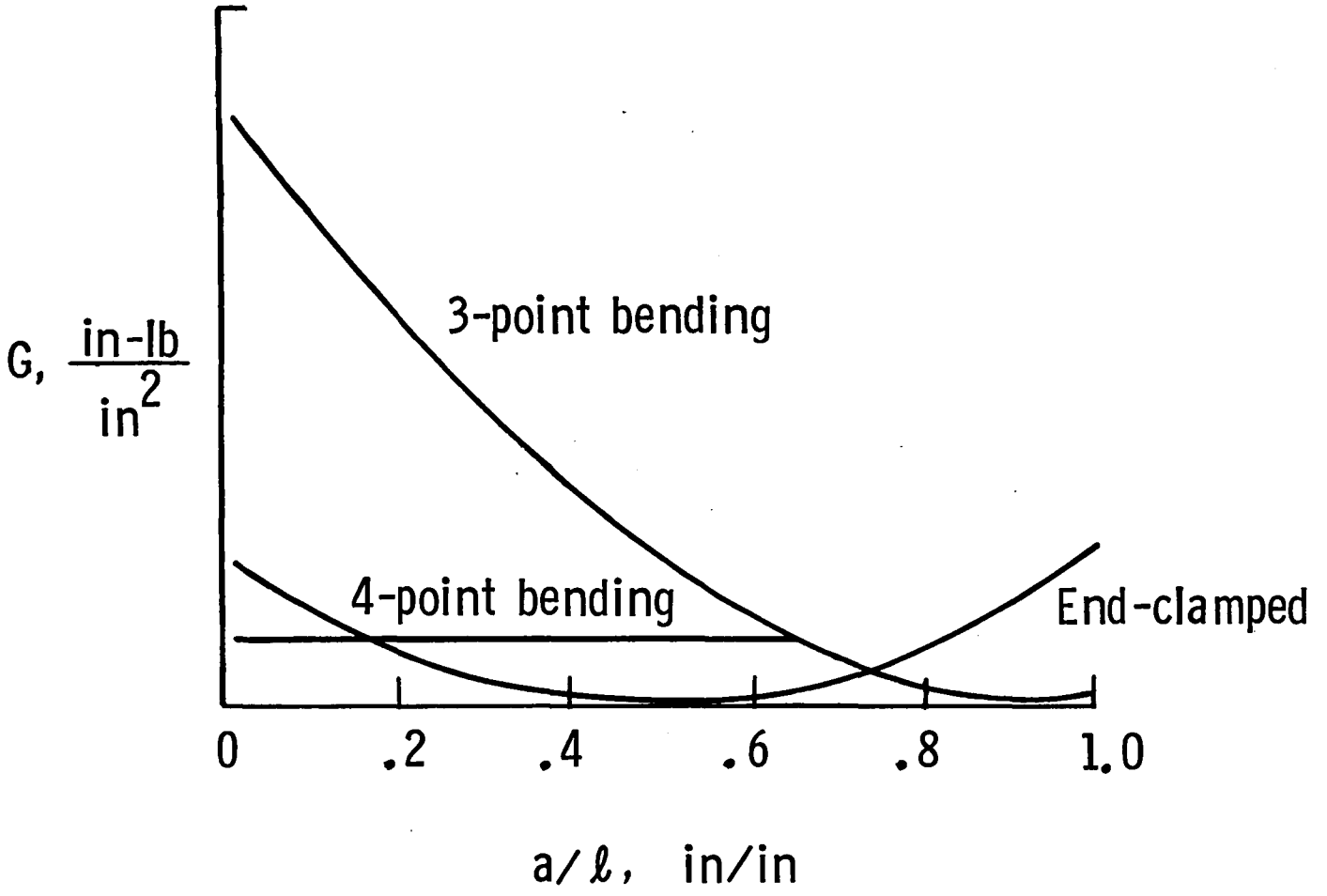

Figure 10. G_c vs. normalized delamination length for three bending configurations.

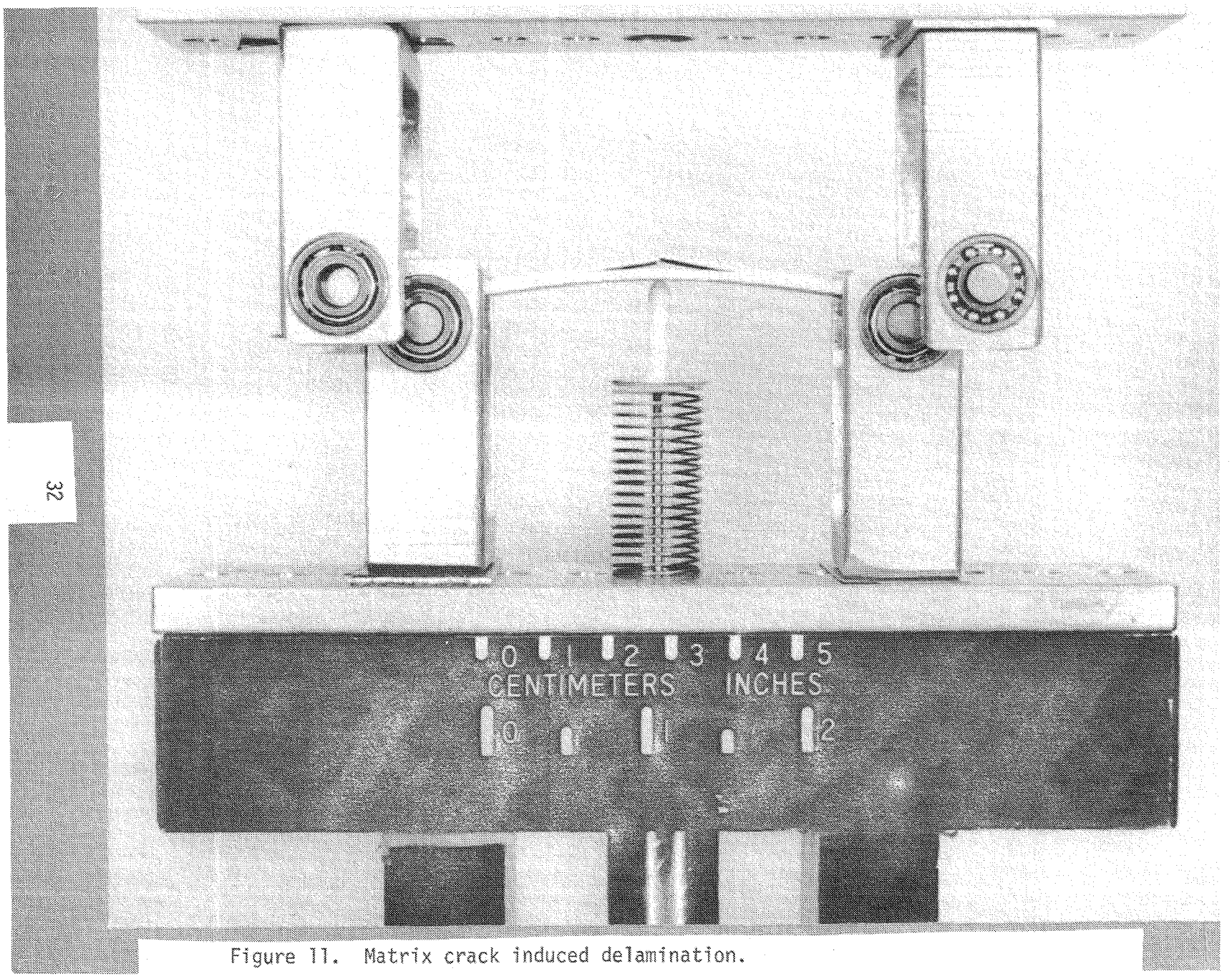

Figure 11. Matrix crack induced delamination.

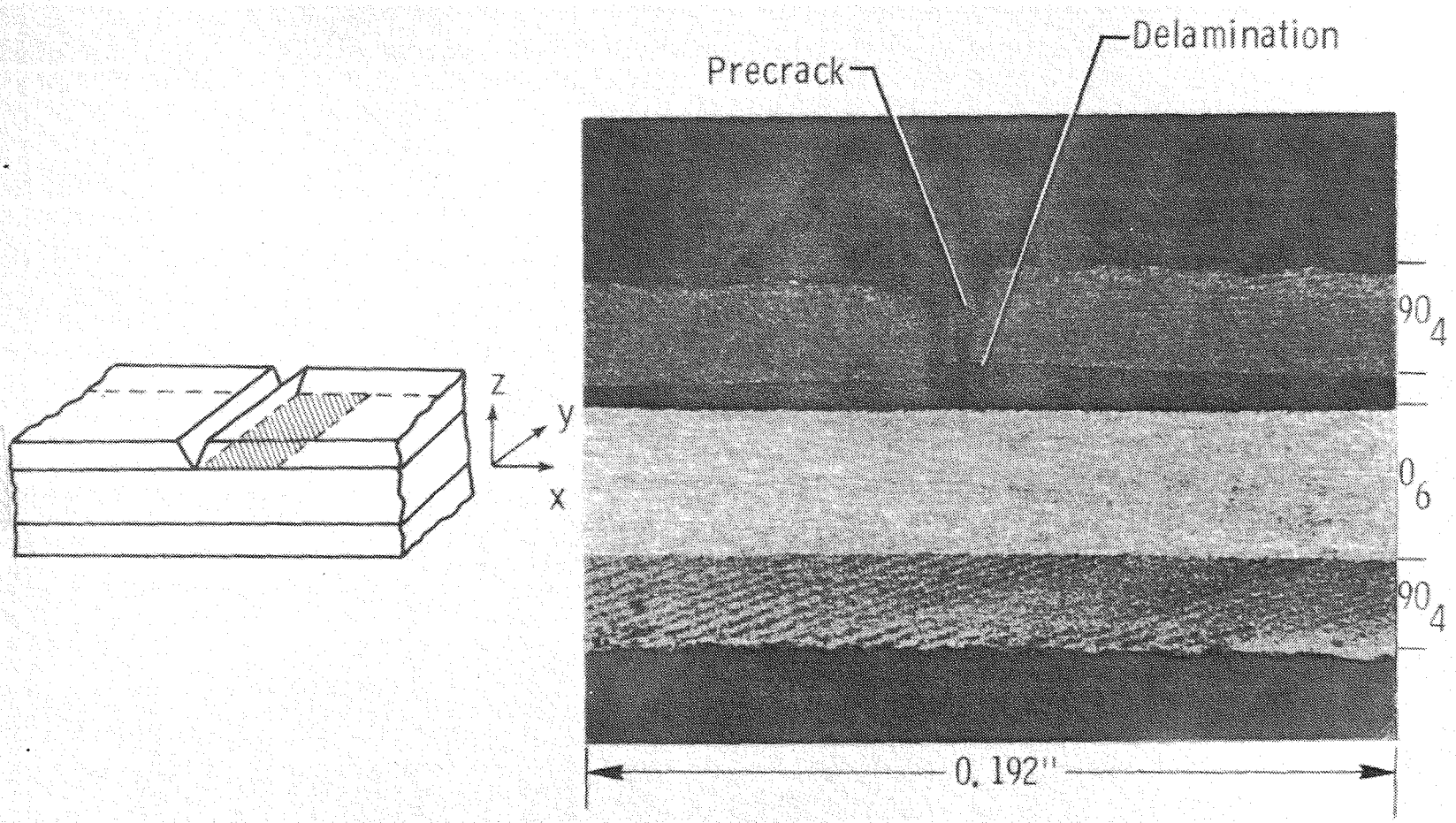

Figure 12. Delaminated [90/0] interface in $[90_4/0_3]_s$ laminate.

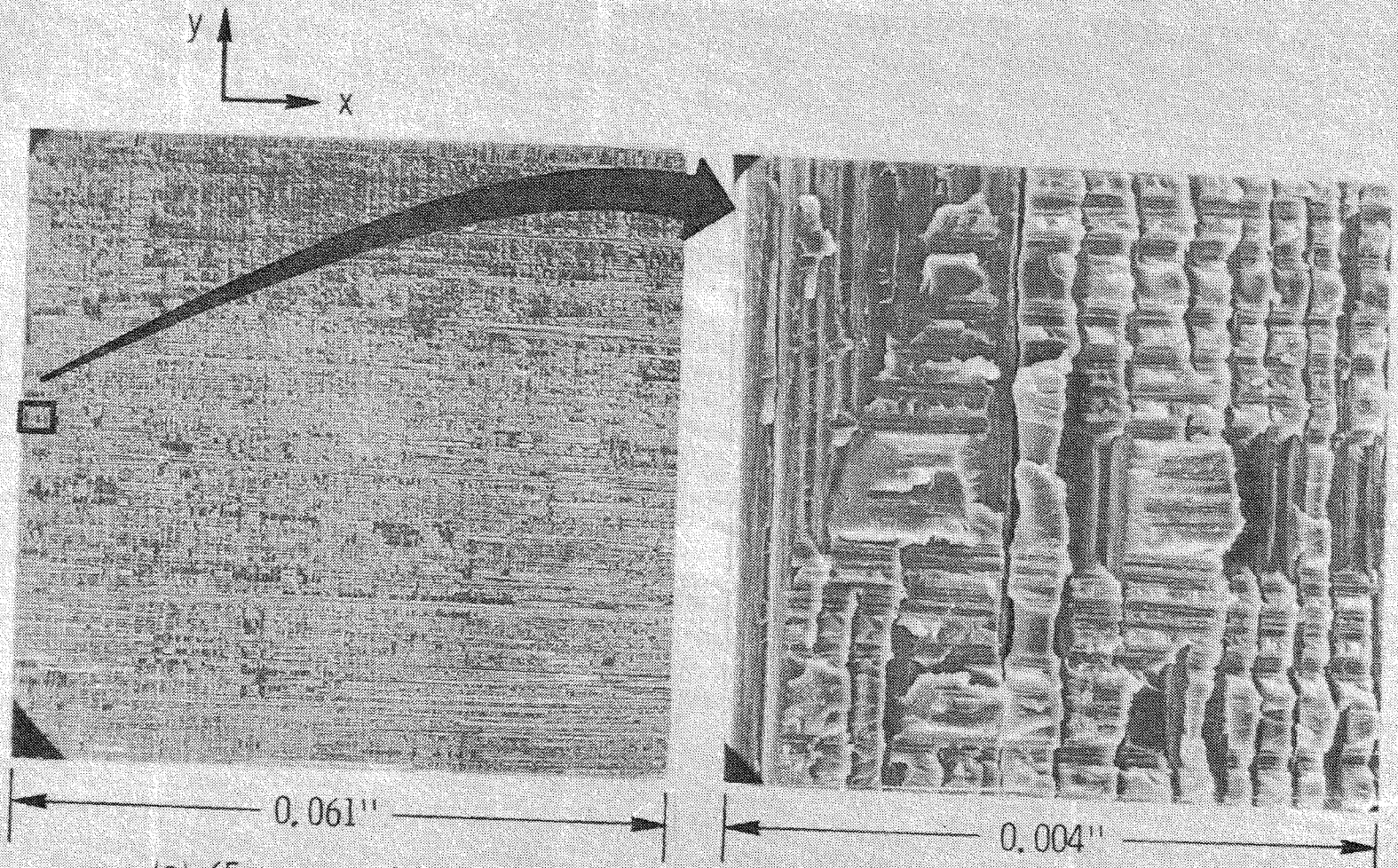

Figure 13. [90/0] failure surface for a $[90_4/0_3]_s$ laminate.

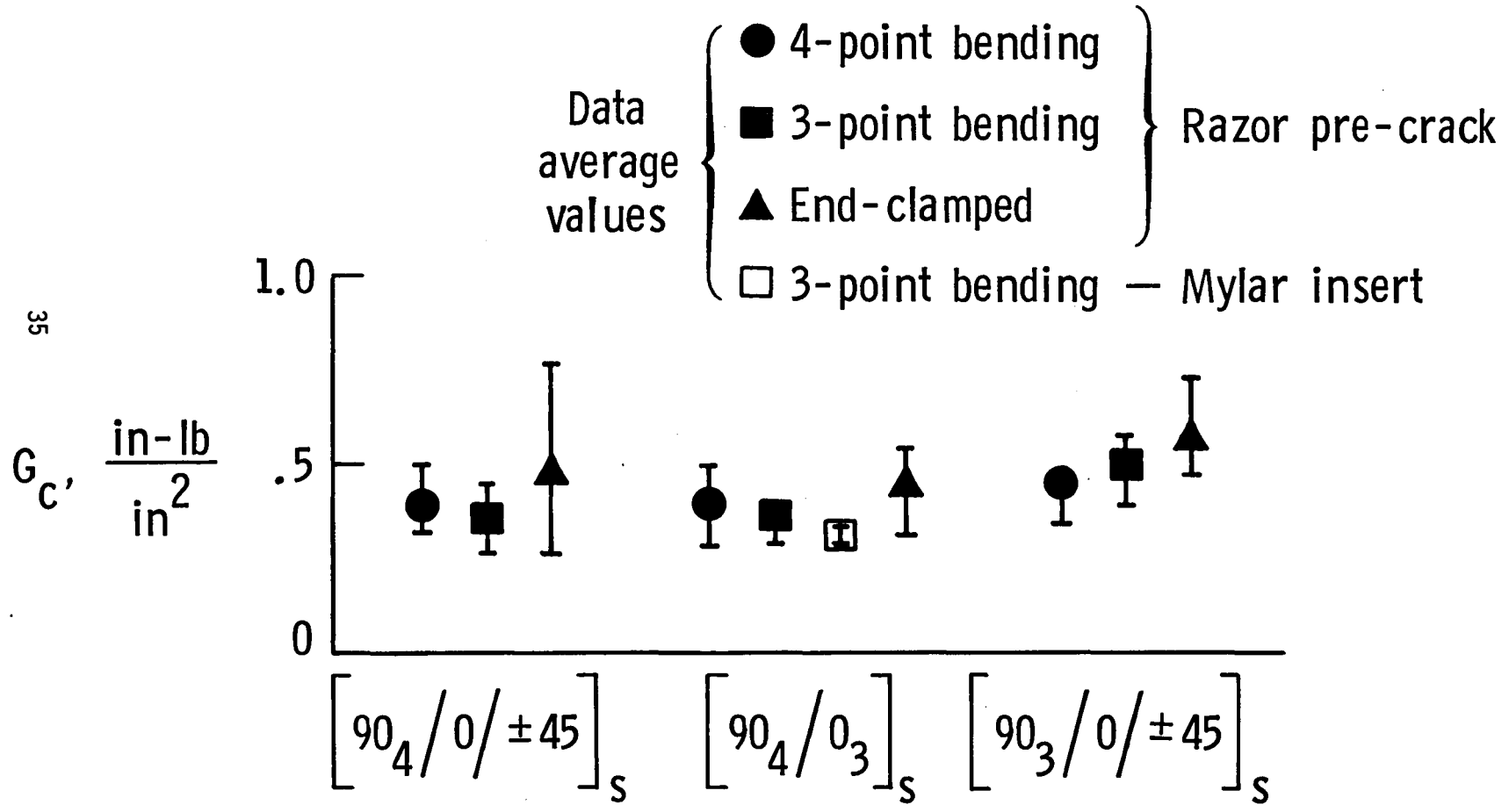

Figure 14. G_c results for three test configurations and three lay-ups.

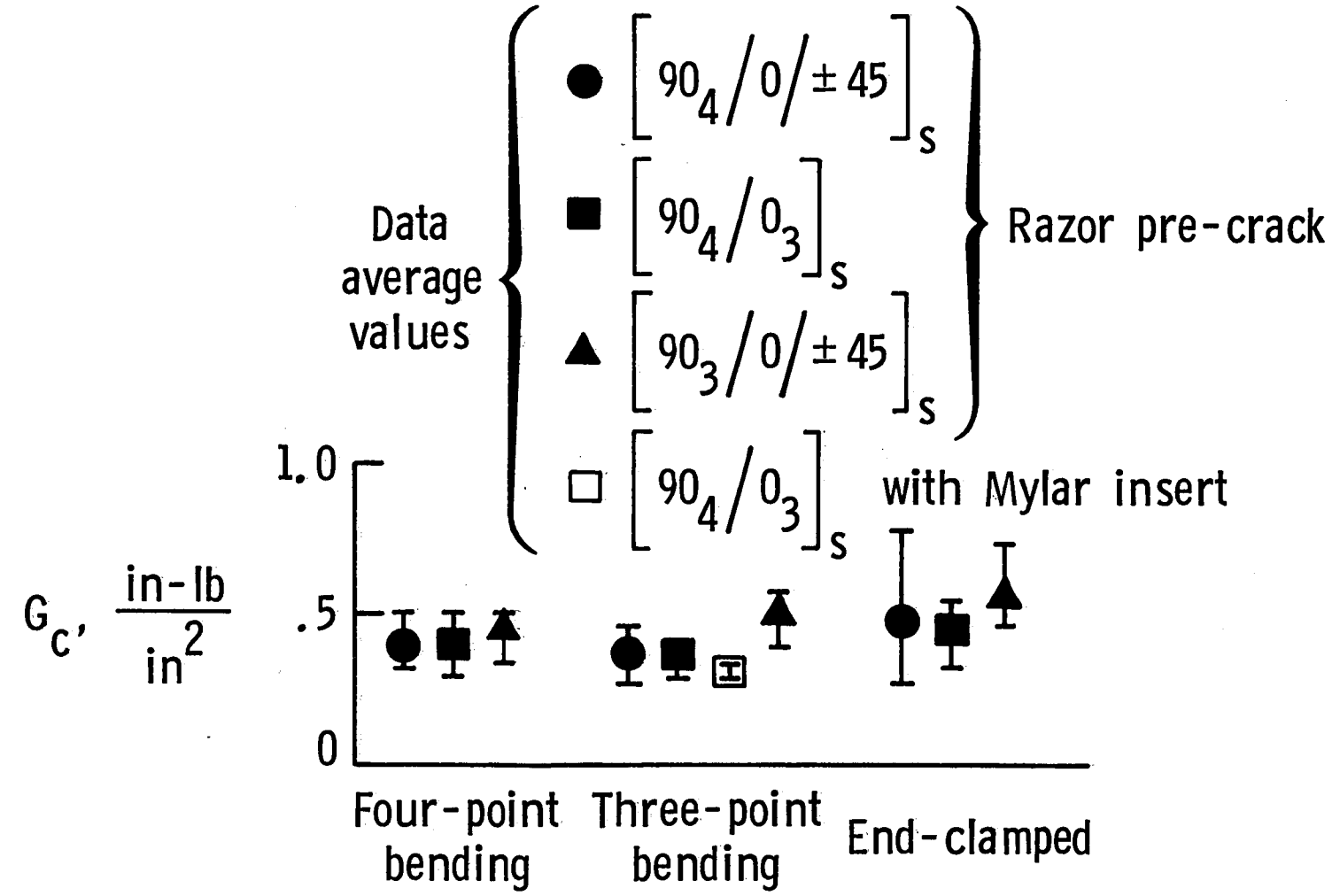

Figure 15. G_c results for three test configurations and three lay-ups.

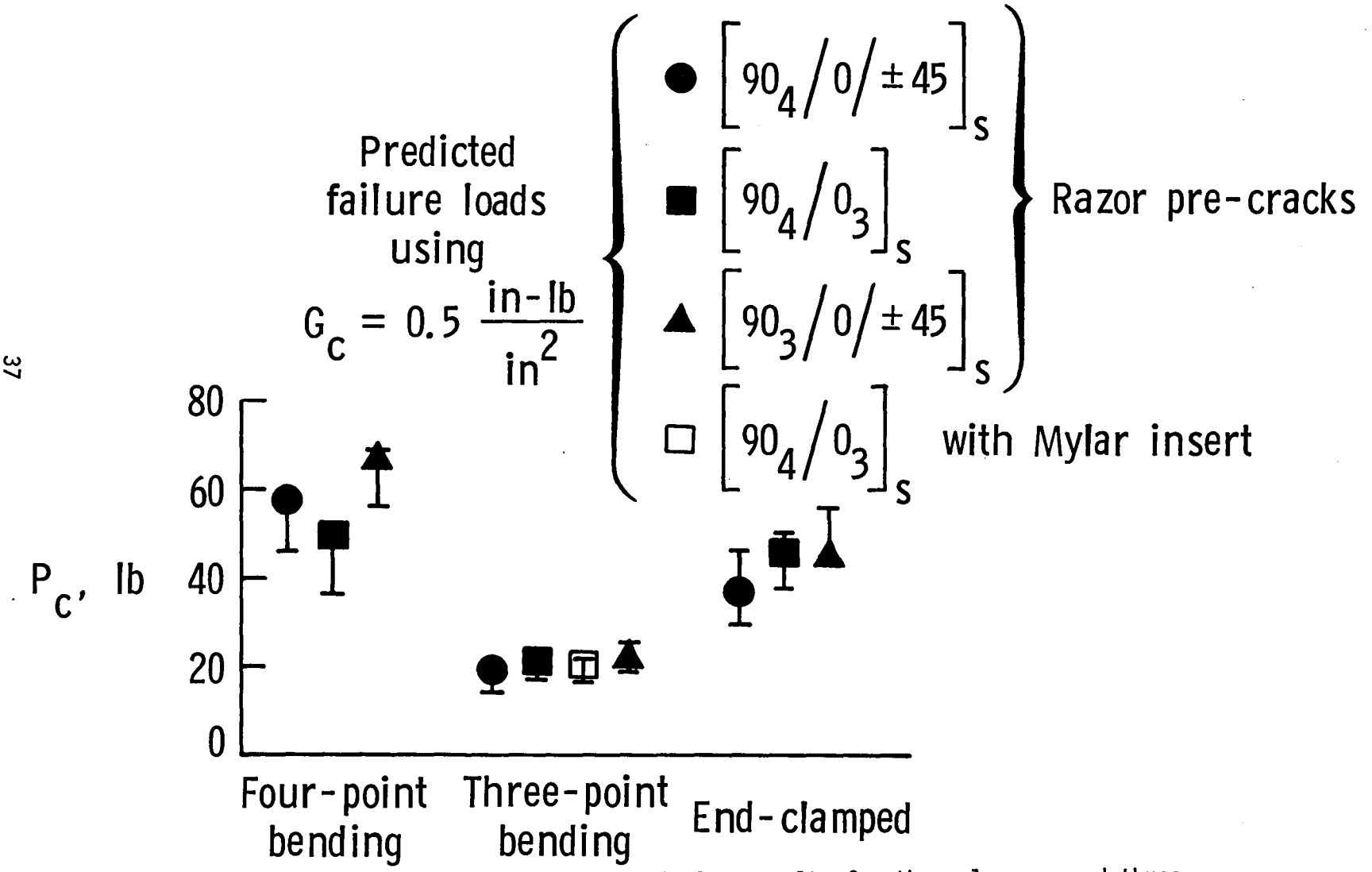

Figure 16. Predicted and measured G_c results for three lay-ups and three bending configurations.

1. Report No NASA TM-87754 USAAVSCOM TM-86-B-2	2. Government Accession No.	3. Recipient's Catalog No.

4. Title and Subtitle Analysis of Delamination Growth from Matrix Cracks in Laminates Subjected to Bending Loads	5. Report Date July 1986 6. Performing Organization Code 506-43-11-04
7. Author(s) Gretchen Bostaph Murri E. Gail Guynn	8. Performing Organization Report No.
9. Performing Organization Name and Address NASA Langley Research Center, Hampton, VA 23665-5225 Aerostructures Directorate, U.S. Army Aviation Research and Technology Activity (AVSCOM), Hampton, VA 23665-5225	10. Work Unit No. 11. Contract or Grant No.
12. Sponsoring Agency Name and Address National Aeronautics and Space Administration Washington, DC 20546 and U.S. Army Aviation Systems Command St. Louis, MO 63166	13. Type of Report and Period Covered Technical Memorandum 14. Army Project No. 1L161102AH45

15. Supplementary Notes

16. Abstract

A major source of delamination damage in laminated composite materials is from low-velocity impact. In thin composite laminates under point loads, matrix cracks develop first in the plies, and delaminations then grow from these cracks at the ply interfaces. The purpose of this study was to quantify the combined effects of bending and transverse shear loads on delamination initiation from matrix cracks. Graphite-epoxy laminates with 90° plies on the outside were used to provide a two-dimensional simulation of the damage due to low-velocity impact. Three plate bending problems were considered: a 4-point bending, 3-point bending, and an end-clamped center-loaded plate. Under bending, a matrix crack will form on the tension side of the laminate, through the outer 90° plies and parallel to the fibers. Delaminations will then grow in the interface between the cracked 90° ply and the next adjacent ply. Laminate plate theory was used to derive simple equations relating the total strain energy release rate, G, associated with the delamination growth from a 90° ply crack to the applied bending load and laminate stiffness properties. Three different lay-ups were tested and results compared. Test results verified that the delamination always formed at the interface between the cracked 90° ply and the next adjacent ply. Calculated values for total G_c from the analysis showed good agreement for all configurations. The analysis was able to predict the delamination onset load for the cases considered. The result indicates that the opening mode component (Mode I) for delamination growth from a matrix crack may be much larger than the component due to interlaminar shear (Mode II).

17. Key Words (Suggested by Author(s)) Composites Delamination Matrix crack Strain energy release rate Bending	18. Distribution Statement Unclassified - Unlimited Subject Category 24

19. Security Classif. (of this report)	20. Security Classif. (of this page)	21. No. of Pages	22. Price*
Unclassified	Unclassified	38	A03

*For sale by the National Technical Information Service, Springfield, Virginia 22161

End of Document